JOURNAL OF GUIDANCE, CONTROL, AND DYNAMICS
Vol. 17, No. 2, March–April 1994

Modeling Hubble Space Telescope Flight Data by Q-Markov Cover Identification

K. Liu* and R. E. Skelton†
Purdue University, West Lafayette, Indiana 47907
and
J. P. Sharkey‡
NASA Marshall Space Flight Center, Huntsville, Alabama 35812

This paper presents a state-space model for the Hubble space telescope under the influence of unknown disturbances in orbit. This model was obtained from flight data by applying the Q-Markov Covariance Equivalent Realization (Q-Markov Cover) identification algorithm. This state-space model guarantees the match of the first Q-Markov parameters and covariance parameters of the Hubble system. The flight data were partitioned into high- and low-frequency components for more efficient Q-Markov Cover modeling to reduce some computational difficulties of the Q-Markov Cover algorithm. This identification revealed more than 20 lightly damped modes within the bandwidth of the attitude control system. Comparisons with the analytical (TREETOPS) model are also included.

I. Introduction

IN its orbit around the Earth, the Hubble space telescope (HST) experiences randomly occurring, unknown, impulse disturbances that are particularly severe upon entering orbit night or orbit day. These disturbances excite the flexible motion of the solar panels causing attitude oscillations of the telescope, making normal operation of the telescope difficult during these periods. The sources of the disturbance are unknown, although it is suspected that they are from thermally induced structural deformations of the solar panel supporting rods (resulting from day heating, night cooling) combined with mechanical stick-slip. In this paper, we present a modal analysis of the telescope flight data using the Q-Markov Covariance Equivalent Realization (Q-Markov Cover) identification algorithm.

To summarize the ideas of the Q-Markov Cover, consider a linear dynamic system, having a state-space realization [A, D, C, H]

$$\begin{aligned} x(k+1) &= Ax(k) + Dw(k) \\ y(k) &= Cx(k) + Hw(k) \end{aligned} \tag{1}$$

where $w(k)$ is the disturbance, $y(k)$ is the telemetric flight data for analysis, and $x(k)$ is the state of the model. We denote n_w, n_y, and n_x as the dimensions of $w(k)$, $y(k)$, and $x(k)$ respectively.

If $x(0) = 0$, and Eq. (1) is excited at its jth disturbance channel with a single unit pulse, then the corresponding response is denoted by $y(j,k)$, where k is the time index. Then, the Markov parameters H_i of the system can be written as

$$H_i = [y(1, i), y(2, i), \ldots, y(n_w, i)], \qquad i = 0, 1, \ldots \tag{2a}$$

and the response to any input $w(k)$ is

$$y(k) = \sum_{i=0}^{k} H_i w(k-i)$$

Therefore, Markov parameters characterize the response of the system. On the other hand, if the system is excited by zero mean white noise at all the disturbance channels, the corresponding response $y(k)$ is a stochastic process, and the correlation R_i can be written as

$$R_i \triangleq \lim_{k \to \infty} E[y(k+i)\, y^*(k)] \qquad i = 0, 1, \ldots \tag{2b}$$

where * denotes matrix transpose (conjugate transpose in the case of a complex matrix). By a slight abuse of language we shall call R_i the "covariance parameters" in terms of the realization (1). The Markov and covariance parameters of a system are

$$H_0 \triangleq H, \qquad H_i \triangleq CA^{i-1}D \qquad i = 1, 2, \ldots \tag{3a}$$

$$R_i \triangleq CA^iXC^* + H_iWH^* \qquad i = 0, 1, 2, \ldots \tag{3b}$$

where matrix X is the solution of the following Lyapunov equation

$$X = AXA^* + DWD^* \tag{3c}$$

where W is the covariance matrix of $w(k)$ when it is white noise.

A Q-Markov Cover of system (1) is defined as follows:

Definition: The state-space model $[\hat{A}, \hat{D}, \hat{C}, \hat{H}]$ is a Q-Markov Cover of system (1) if

$$\hat{H}_i = H_i \quad \text{and} \quad \hat{R}_i = R_i \qquad i = 0, 1, \ldots, Q-1 \qquad \square$$

The Q-Markov Cover identification algorithm was developed from the Q-Markov Cover theory of model reduction.[2,5,6] The identification algorithm produces state-space models that match the first Q-Markov and covariance parameters (H_i, R_i, $i = 0, \ldots, Q-1$) of the actual system generating the output data. The algorithm has been applied to NASA's MINIMAST large flexible structure at the NASA Langley Research Center and to the ACES structure at the NASA Marshall Space Flight Center to obtain state-space models for controller design.[7,10] Controllers designed from the identified models were implemented on MINIMAST and ACES and are described in Refs. 7 and 10.

To get good models in both the low- and high-frequency spectrum and to avoid certain computational difficulties of the Q-Markov Cover (to be discussed later), we use two different frequency weightings, yielding two different models. The two models are then combined (and reduced) to produce the final model. The first frequency weighting is a lowpass filter, passing only frequen-

Received Sept. 19, 1991; revision received Feb. 27, 1993; accepted for publication May 3, 1993.

*Research Assistant, School of Aeronautics and Astronautics.
†Director, Space Systems Control Laboratory. Fellow AIAA.
‡Deputy Branch Chief. Member AIAA.

cies up to 0.25 Hz. The second frequency weighting passes only frequencies beyond 0.25 Hz.

The paper is organized as follows. Sec. II describes the formulas of the Q-Markov Cover identification algorithm. Sec. III discusses flight data and the necessity of frequency weighting. The Q-Markov Cover algorithm with frequency partitioning (weighting) is presented in Sec. IV. The modal analysis of the Q-Markov Cover results of the flight data are presented in Sec. V. Section VI contains a brief conclusion.

II. Deterministic Q-Markov Cover Identification

There are two versions of the Q-Markov Cover identification algorithm, a deterministic version and a stochastic version, both presented in Ref. 7. We only describe the deterministic version in this section.

The deterministic Q-Markov Cover identification algorithm obtains Q-Markov Covers of a system from the pulse response of the system. Assume now that system (1) is excited by a single pulse input. Write the single pulse input $w(j,k)$ as

$$w(j,k) \triangleq w_j \delta_{ok} \tag{4a}$$

where δ_{ok} is the Kroneker delta and w_j is the magnitude of the single pulse. Define the matrix of pulse magnitudes squared as

$$W \triangleq \text{diag}[\ldots w_j^2 \ldots] \tag{4b}$$

Then the pulse response data $y(j,k), j = 1, 2, \ldots, n_w$ and $k = 0, 1, \ldots, d$ are the data used by the identification algorithm to generate Q-Markov Covers, where d is the decay time of the transient response.

It has been shown in Ref. 7 that the covariance parameters R_i in Eq. (2b) have deterministic interpretation given by

$$R_i = \lim_{d\to\infty} R_{d_i}, \quad R_{d_i} \triangleq \sum_{j=1}^{n_w}\sum_{k=0}^{d} y(j,k+i)\, y^*(j,k) \qquad i = 0, 1, \ldots \tag{5a}$$

and, as before,

$$H_i \triangleq [y(1,i), y(2,i), \ldots, y(n_w,i)]\, W^{-1/2}, \quad i = 0, 1, \ldots \tag{5b}$$

The following is the computational procedure of the Q-Markov Cover identification algorithm.

Form the following Toeplitz matrices $\boldsymbol{R}_Q$ and $\boldsymbol{H}_Q$ with the first Q impulse response parameters H_i, $i = 0, 1, \ldots, Q$-1, and the first Q deterministic covariance parameters R_{d_i}, $i = 0,1, \ldots, Q-1$:

$$\boldsymbol{R}_Q \triangleq \begin{bmatrix} R_{d_0} & R_{d_1}^* & \cdots & R_{d_{Q-1}}^* \\ R_{d_1} & R_{d_0} & \cdots & \\ \cdots & & \ddots & \\ R_{d_{Q-1}} & & \cdots & R_{d_0} \end{bmatrix} \boldsymbol{R}_Q \in \Re^{n_y Q \times n_y Q} \tag{6a}$$

$$\boldsymbol{H}_Q \triangleq \begin{bmatrix} H_0 & 0 & \cdots & 0 \\ H_1 & H_0 & \cdots & 0 \\ \vdots & \vdots & \ddots & \vdots \\ H_{Q-1} & H_{Q-2} & \cdots & H_0 \end{bmatrix} \boldsymbol{H}_Q \in \Re^{n_y Q \times n_w Q} \tag{6b}$$

Define also a block column matrix $\boldsymbol{M}_Q$ with the $Q-1$ pulse response parameters H_i $i = 1, \ldots, Q-1$

$$\boldsymbol{M}_Q = \begin{bmatrix} H_1 \\ H_2 \\ \vdots \\ H_{Q-1} \end{bmatrix} \tag{6c}$$

Define the data matrix $\boldsymbol{D}_Q$ formed by

$$\boldsymbol{D}_Q = \boldsymbol{R}_Q - \boldsymbol{H}_Q \overline{W} \boldsymbol{H}_Q^* \tag{6d}$$

where $\overline{W} \triangleq \text{diag}[\ldots \text{W} \ldots] \in \Re^{n_y Q \times n_w Q}$.

With the matrices $\boldsymbol{D}_Q$, $\boldsymbol{M}_Q$, and H_0, we can proceed with the Q-Markov Cover computation as follows: Compute $\boldsymbol{P}_Q$, a full column rank matrix factor of the data matrix $\boldsymbol{D}_Q$. Hence

$$\boldsymbol{D}_Q = \boldsymbol{P}_Q \boldsymbol{P}_Q^* \quad \boldsymbol{P}_Q \text{ full column rank} \in \Re^{n_y Q \times \hat{n}_x} \tag{7}$$

where $\hat{n}_x = \text{rank}\,(\boldsymbol{D}_Q)$. Partition $\boldsymbol{P}_Q$ matrix as

$$\boldsymbol{P}_Q = \begin{bmatrix} P_0 \\ \bar{\boldsymbol{P}} \end{bmatrix} = \begin{bmatrix} \boldsymbol{P} \\ P_{Q-1} \end{bmatrix}, \quad P_0, P_{Q-1} \in \Re^{n_y \times n_x}$$
$$\boldsymbol{P}, \bar{\boldsymbol{P}} \in \Re^{[n_y(Q-1)] \times \hat{n}_x} \tag{8}$$

Let $V_p \in \Re^{\hat{n}_x \times (\hat{n}_x - r)}$ denote a unitary basis for the nullspace of $\boldsymbol{P}$ where $r = \text{rank}\,(\boldsymbol{P})$. Let $V_{\bar{P}} \in \Re^{(\hat{n}_x + n_w) \times (\hat{n}_x - r)}$ denote a unitary basis for the nullspace of $[\bar{\boldsymbol{P}}\ \boldsymbol{M}_Q]$. Then the SVD of $\boldsymbol{P}$ and $[\bar{\boldsymbol{P}}\ \boldsymbol{M}_Q]$ may be written in the form

$$P = U_p \begin{bmatrix} \Sigma_p & 0 \\ 0 & 0 \end{bmatrix} \begin{bmatrix} V_{p_1}^* \\ V_p \end{bmatrix}, \quad [\bar{\boldsymbol{P}}\ \boldsymbol{M}_Q] = U_{\bar{p}} \begin{bmatrix} \Sigma_{\bar{p}} & 0 \\ 0 & 0 \end{bmatrix} \begin{bmatrix} V_{\bar{p}_1}^* \\ V_{\bar{p}}^* \end{bmatrix} \tag{9}$$

The following equations parameterize *all* Q-Markov Covers by matrices $[\hat{A}, \hat{D}, \hat{C}, \hat{H}]$:

$$[\hat{A}, \hat{D}] = \boldsymbol{P}^+ [\bar{\boldsymbol{P}}, \boldsymbol{M}_Q] + V_{\bar{P}} U V_{\bar{P}}^* \begin{bmatrix} I & 0 \\ 0 & W^{-1/2} \end{bmatrix}$$
$$\hat{C} = P_o \tag{10}$$
$$\hat{H} = H_o$$

where $U \in \Re^{(\hat{n}_x - r) \times (\hat{n}_x + n_w - r)}$ is an arbitrary row unitary matrix.

If the parameter d in Eq. (5a) approaches infinity, the matrices $[\hat{A}, \hat{D}, \hat{C}, \hat{H}]$ in Eq. (10) represent all the stable minimal Q-Markov Covers of system (1) with matrix U as a free parameter[7] (see also Ref. 6). Hence the Q-Markov Cover of a system is not unique. But if the matrix $\boldsymbol{P}$ is full rank, then the Q-Markov Cover calculated by Eq. (10) is unique since $V_p = 0$.

There are two parameters to be set in the Q-Markov Cover identification algorithm: the parameter Q, the number of Markov parameters and covariance parameters to be matched, and the numerical zero threshold ε needed for rank test of matrix $\boldsymbol{D}_Q$ in its full rank factorization, Eq. (7), and the rank test of matrix $\boldsymbol{P}$. Practically, the upper bound of the parameter Q is determined by the computational limitations of the computer for the matrix factorization (7). (The size of $\boldsymbol{D}_Q$ grows linearly with the increase of Q.) One rule of thumb for the lowest selection of Q is the number of data samples in a complete period of the lowest frequency in the data. The choice of the numerical zero threshold ε is determined by the reliability of the numerical computation and the signal-to-noise ratio of the available data. When the data are very noisy, choosing a larger threshold ε may reduce noise effects on the identified model. The disadvantage of a relatively large rank test threshold ε is an inexact matching of the first Q-Markov parameters and first Q

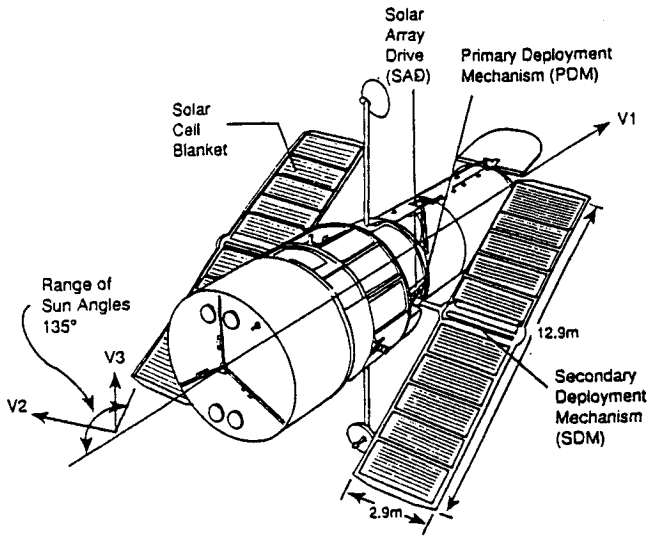

Fig. 1 HST on-orbit deployed configuration.

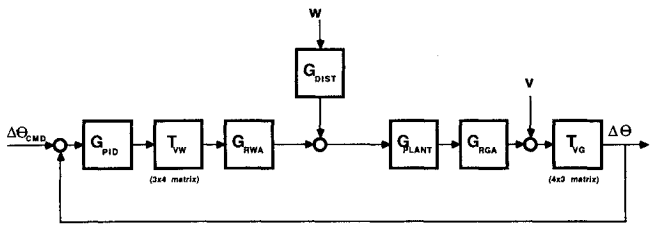

Fig. 2 System ID model: plant + disturbance + controller. [Note that there are three 40 Hz modes of operation (as of March 29, 1991): a) low bandwidth P-D "maneuver gains" (0.15 Hz), b) high bandwidth P-D "acquisition gains" (0.75 Hz), and c) high bandwidth P-I-D "science gains with 1 Hz observer. All data presented there used maneuver gains.]

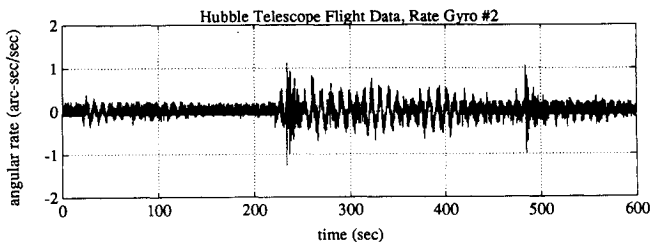

Fig. 3 Flight data, hour 6, day 143.

covariance parameters. An advantage of a large ε is the averaging effects this has on the noisy data. When ε is set very small, the resulting model order $\hat{n}_x$ from the rank test of $\boldsymbol{D}_q$ will be high. Some of the noise characteristics will be captured by an identified model and be represented by some modes (commonly called noise modes) in the model.[10] By further analysis, these noise modes can be extracted and eliminated.[10] Hence, proper choice of threshold value ε is important when data is noisy. At this point, the choice of ε is largely trial and error.

III. HST Flight Data and its Frequency Partition

The data used in the following analyses were obtained under closed-loop conditions of the HST in an attitude hold mode. Figure 1 provides a pictorial description of the HST and designates the vehicle coordinate system as used within the attitude control law. The two solar arrays, shown at an angle of 45 deg with respect to the *V2-V3* plane, can rotate independently during spacecraft attitude maneuvers but are held in place by a brake mechanism in the attitude hold mode. A preflight simulation model of the HST, using

Table 1 TREETOPS simulation model of the HST

Summary of TREETOPS component modes			
Component	Description	Number of modes	Frequency range
Body 1	SSM/OTA	6 RDOF	0 Hz
Body 2	+V2 solar array	21 FDOF	0.1–5.5 Hz
Body 3	−V2 solar array	21 FDOF	0.1–5.5 Hz
Body 4	+HGA boom	3 FDOF	0.43–2.8 Hz
Body 5	−HGA boom	3 FDOF	0.43–2.8 Hz
Body 6	+HGA X gimbal	1 RDOF	0 Hz
Body 7	−HGA X gimbal	1 RDOF	0 Hz
Body 8	+HGA Y gimbal & ant.	1 RDOF	0 Hz
Body 9	−HGA Y gimbal & ant.	1 RDOF	0 Hz
Body 10	Aperture door	1 FDOF	0.91 Hz
Actuators	4 reaction wheels	4 −2nd order	50 Hz
Sensors	4 rate gyros	4 −2nd order	18 Hz
Controller	PID/FIR w/delay	12 −2nd order	0–10 Hz
Total		79 2nd order "modes" (158 states)	

NASA's TREETOPS program, is summarized in Table 1. Note that the structural design of the HST attributes all flexible modes under 10 Hz to the flexible appendages [solar arrays, high gain antenna (HGA) and aperture door]. A simplified block diagram of this system with external disturbances is shown in Fig. 2. There are six integrating-rate gyro assemblies (RGAs) on the HST, located on the back side of the optical telescope assembly in a skewed configuration. The control system may use combinations of three or four of these gyros to derive vehicle rates using the [Tvg] transformation. These vehicle rates are then used in a classical single-input/single-output (SISO) proportional + integral + derivative (PID) compensator to derive the four reaction wheel assemblies (RWA) via the [Tvw] transformation. This compensator was designed for a 40 Hz sample rate with the assumption that the disturbances to the flexible appendages would be dominated by the RWA torques. Upon request, the onboard telemetry system can transmit both RGA data (16 bits; 1 LSB = 0.005 arcsec/s) and RWA data (24 bits) at 40 Hz to the ground. Not shown are additional control subsystems for command feedforward, momentum management, gravity-gradient compensation, HGA control, etc.

Figure 3 shows a segment of telemetry data from rate gyro 2 when the telescope entered from orbit night to orbit day. The data were received in the sixth hour of day 143 of the calendar year 1990. The sudden burst of oscillation appearing in the middle of the data segment was caused by an unknown disturbance. This was the data set used for our analysis. Figure 4 shows the portion of the data used for rate gyro 2, which is the data portion starting from 233.55 ending at 483.4755 of the data in Fig. 3.

To model the telescope response to the unknown disturbance, we assume that the disturbance can be modeled deterministically by the following state-space equation:

$$x_w(k+1) = A_w x_w(k) + D_w w(k)$$
$$y_w(k) = C_w x_w(k) \tag{11}$$

where $w(k)$ is a scalar single unit pulse and $y_w(k)$ is the actual disturbance acting on the telescope, that is, $w(k) = \delta_{ok} \in \Re$ and $y_w(k) \in \Re^{n_{y_w}}$ with n_{y_w} unknown. We assume the response of the telescope to the disturbance can be described by the equation

$$x_h(k+1) = A_h x_h(k) + D_h y_w(k)$$
$$y(k) = C_h x_h(k) + H_h y_w(k) \tag{12}$$

where $y(k) \in \Re^4$ are the rate gyro measurements. Based on physical modeling principals, $H_h = 0$ for the telescope. Then the tele-

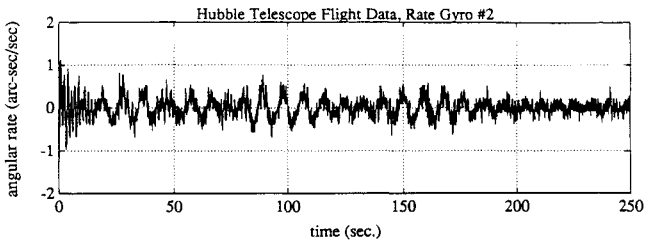

Fig. 4 Disturbance response of the flight data.

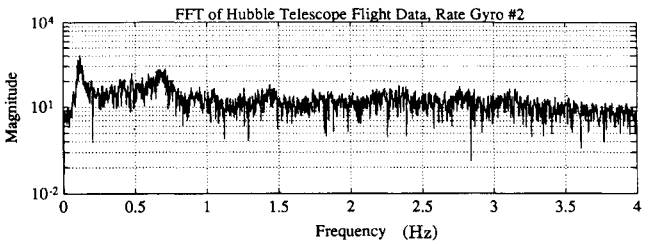

Fig. 5 Fourier transformation of the disturbance response.

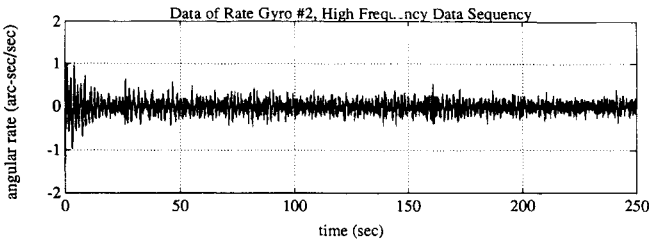

Fig. 6 Disturbance response of the high-frequency weighted data.

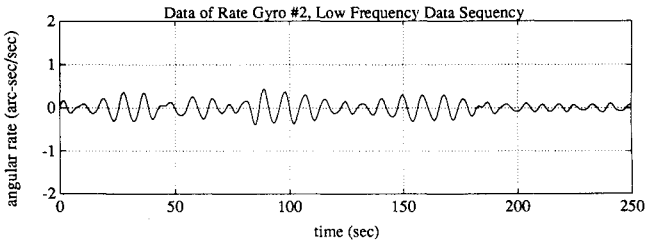

Fig. 7 Disturbance response of the low-frequency weighted data.

scope response to the unknown disturbance can be described by

$$x(k+1) = Ax(k) + Dw(k)$$
$$y(k) = Cx(k) + Hw(k) \tag{13}$$

where

$$A = \begin{bmatrix} A_h & D_h C_w \\ 0 & A_w \end{bmatrix}, \quad D = \begin{bmatrix} 0 \\ D_w \end{bmatrix}, \quad C = [C_h \quad 0], \quad H = 0 \tag{14}$$

Therefore, the telescope oscillatory response to the disturbance (such as the data segment shown in Fig. 4) can be modeled by state-space Eq. (13) with a single unit pulse input. The identification problem is now reduced to the problem of identifying the telescope state-space model [Eq. (13)] by assuming a unit pulse as the input.

It can be easily observed from the data in Fig. 4 that the envelope of the disturbance response has a period of nearly 100 s. A direct application of the Q-Markov Cover would be computationally difficult because of the size of the data set. To achieve a good identification, we need to choose the Q parameter larger than 4000 (which is the envelope period times the sampling rate). This choice results in a $\boldsymbol{D}_Q$ matrix that is 16,000 by 16,000. But the dimension of $\boldsymbol{D}_Q$ that can be reliably factored by our computer is about 600. We could reduce the sampling rate to reduce the value of Q, but this reduction would introduce severe aliasing of the high-frequency components of the data, many of which may be important to the model.

To simplify the computation we identified the low- and high-frequency components separately. A low-frequency data set is obtained by eliminating high-frequency components from the data. Hence, a lower sampling rate can be used on the low-frequency data set. By decimating the data, we used a higher sampling rate on the higher frequency identification and a lower sampling rate on lower frequency identification. This method generated a Q-Markov Cover model for each of two frequency bands. The combined model was formed by assembling both models together.

Figure 5 shows the magnitude of the discrete fourier transform of the data from rate gyro 2. The low-frequency components of the data were concentrated around 0.12 Hz, and the high-frequency components were above 0.35 Hz. There is a natural separation at 0.25 Hz. We chose this frequency for separating the high-frequency components from the low-frequency components of the data. We then partitioned the data into its low-frequency component and high-frequency component. For rate gyro 2, the inverse transform of the high-frequency and low-frequency portions of the data are shown in Figs. 6 and 7, respectively.

From Fig. 7, we can see that the beating period of the low-frequency portion of the data is nearly 100 s. For example, if 4 Hz is chosen to be the sampling rate for this data, one must choose Q larger than 400 to capture this 100 s period. The resulting $\boldsymbol{D}_Q$ matrix will have a dimension larger than 1600×1600. Higher sampling rates will result in even larger dimensions for $\boldsymbol{D}_Q$ (whose dimension is $n_y Q \times n_y Q$), because there are more samples in one period. To obtain a higher sampling rate and to reduce the size of the $\boldsymbol{D}_Q$ matrix, we identified models for systems using each of the four output signals separately. Assume that $[\hat{A}_{lf1}, \hat{D}_{lf1}, \hat{C}_{lf1}, \hat{H}_{lf1}]$ is the obtained Q-Markov Cover model for ith output signal. The complete low-frequency model $[\hat{A}_{lf}, \hat{D}_{lf}, \hat{C}_{lf}, \hat{H}_{lf}]$ for all four rate gyros was obtained by combining the four identified single-output Q-Markov Cover models. The complete model is then in the following form:

$$\hat{A}_{lf} = \begin{bmatrix} \hat{A}_{lf1} & 0 & 0 & 0 \\ 0 & \hat{A}_{lf2} & 0 & 0 \\ 0 & 0 & \hat{A}_{lf3} & 0 \\ 0 & 0 & 0 & \hat{A}_{lf4} \end{bmatrix}, \qquad \hat{D}_{lf} = \begin{bmatrix} \hat{D}_{lf1} \\ \hat{D}_{lf2} \\ \hat{D}_{lf3} \\ \hat{D}_{lf4} \end{bmatrix}$$

$$\hat{C}_{lf} = \begin{bmatrix} \hat{C}_{lf1} & 0 & 0 & 0 \\ 0 & \hat{C}_{lf2} & 0 & 0 \\ 0 & 0 & \hat{C}_{lf3} & 0 \\ 0 & 0 & 0 & \hat{C}_{lf4} \end{bmatrix}, \hat{D}_{lf} = \begin{bmatrix} \hat{D}_{lf1} & 0 & 0 & 0 \\ 0 & \hat{D}_{lf2} & 0 & 0 \\ 0 & 0 & \hat{D}_{lf3} & 0 \\ 0 & 0 & 0 & \hat{D}_{lf4} \end{bmatrix}$$

This model is apparently overparameterized (is not a minimal realization). Balanced model reduction (an arbitrary choice) is applied to reduce the size of this model.

IV. Q-Markov Cover Identification Algorithm with Frequency Partitioned Data

When the data are frequency weighted and modeled by Q-Markov Covers at a different sampling rate for each weight, we may combine the models into a single model at the original sampling rate. This model is a simple algebraic problem. The order of

this model must be reduced because a simple combination of the models may not be minimal. The process is described as follows. Suppose a continuous system is sampled at two different rates. Call the original sample period T_o and the new sample period T_n. Suppose, at sample rate T_o^{-1}, the discrete state-space model obtained is $[A_o, D_o, C_o, H_o]$, and at new sample rate T_n^{-1}, the discrete state-space model obtained is $[A_n, D_n, C_n, H_n]$. Then, assuming a zero-order hold, the two sets of matrices can be related by the following algebraic equation, with some matrices A_c and D_c:

$$A_o = e^{A_c T_o}$$

$$A_n = e^{A_c T_n}$$

$$D_o = \int_o^{T_o} e^{A_c(T_o - t)} dt D_c \tag{15}$$

$$D_n = \int_o^{T_n} e^{A_c(T_n - t)} dt D_c$$

$$C_o = C_n, \qquad H_o = H_n$$

Therefore, conversion of the model at sampling rate T_n^{-1} to a model at the original sampling rate T_o^{-1} can be done by solving for the matrices $[A_o, D_o, C_o, H_o]$ in Eq. (15), given matrices $[A_n, D_n, C_n, H_n]$. The solution routine is straightforward in MATLAB.[10]

Suppose the fourier transform of the original data $y(k)$ is weighted with n_f different frequency weights (stop bands) yielding n_f different time series $y_i(k)$, $i = 1, 2, \ldots, n_f$. By applying the Q-Markov Cover identification algorithm to each data set separately, we obtain n_f Q-Markov Cover models described by the following matrices for each data set, respectively:

$$[\hat{A}_i, \hat{D}_i, \hat{C}_i, \hat{H}_i], \qquad i = 1, 2, \ldots, n_f \tag{16}$$

Since

$$y(k) = y_1(k) + y_2(k) + \ldots + y_{n_f}(k) \tag{17}$$

we can obtain a model $[\hat{A}, \hat{D}, \hat{C}, \hat{H}]$ for the original data $y(k)$ by combining the n_f Q-Markov Cover models in parallel

$$\hat{A} = \operatorname{diag}\left[\hat{A}_1, \ldots, \hat{A}_{n_f}\right]$$

$$D = \begin{bmatrix} \hat{D}_1 \\ \vdots \\ \hat{D}_{n_f} \end{bmatrix} \tag{18}$$

$$\hat{C} = \left[\hat{C}_1, \ldots, \hat{C}_{n_f}\right], \qquad \hat{H} = \operatorname{diag}\left[\hat{H}_1, \ldots, \hat{H}_{n_f}\right]$$

The combined model [Eq. (18)] is usually not minimal. The pole-zero cancellations can be eliminated by an ordinary model reduction process. Some of the effective model reduction algorithms for this purpose include component cost analysis,[1,4] PQ projection,[3] balance coordinates,[8] etc.

Hence, the algorithm for Q-Markov Cover identification with frequency partitioning of data can be summarized as follows:

Step 1: Apply different weights (stop bands) to the fourier transforms of the original data. Denote the different time series of each weighted data set by $y_i(k)$, $i = 1, 2, \ldots, n_f$. Obtain new data $\hat{y}_i(k)$, $i = 1, 2, \ldots, n_f$ from $y_i(k)$, $i = 1, 2, \ldots, n_f$ by decimating at new sampling frequencies f_i, $i = 1, 2, \ldots, n_f$.

Step 2: Apply the Q-Markov Cover identification algorithm individually to each data set $\hat{y}_i(k)$, $i = 1, 2, \ldots, n_f$ to obtain the Q-Markov Covers $[A_i, D_i, C_i, H_i]$, $i = 1, 2, \ldots, n_f$.

Step 3: Solve Eq. (15) to convert the models obtained in step 2 at different sampling frequencies to the models at original sampling frequency. Assume that the model for the ith data set at the original sampling frequency is $[\hat{A}_i, \hat{D}_i, \hat{C}_i, \hat{H}_i]$, $i = 1, 2, \ldots, n_f$.

Step 4: Form the augmented model $[\hat{A}, \hat{D}, \hat{C}, \hat{H}]$ according to Eq. (18) using models $[\hat{A}_i, \hat{D}_i, \hat{C}_i, \hat{H}_i]$, $i = 1, 2, \ldots, n_f$.

Step 5: Reduce model $[\hat{A}, \hat{D}, \hat{C}, \hat{H}]$ to obtain a final model for the original data $y(k)$.

V. Modeling Results of HST Data

As discussed in Sec. III, the flight data were partitioned into low-frequency and high-frequency components. The data sets were then identified separately by the Q-Markov Cover algorithm. The final model was computed by connecting the two Q-Markov Cover models in parallel and reducing the resulting model by a balanced reduction method, in MATLAB.

Identifying the high-frequency data set is a straightforward computation of a Q-Markov Cover. The period of the lowest frequency of this data set (below 0.24 Hz) is about 4 s. Hence, $Q = 160$ was used. This choice results in a 640×640 matrix $\boldsymbol{D}_Q$. High-frequency

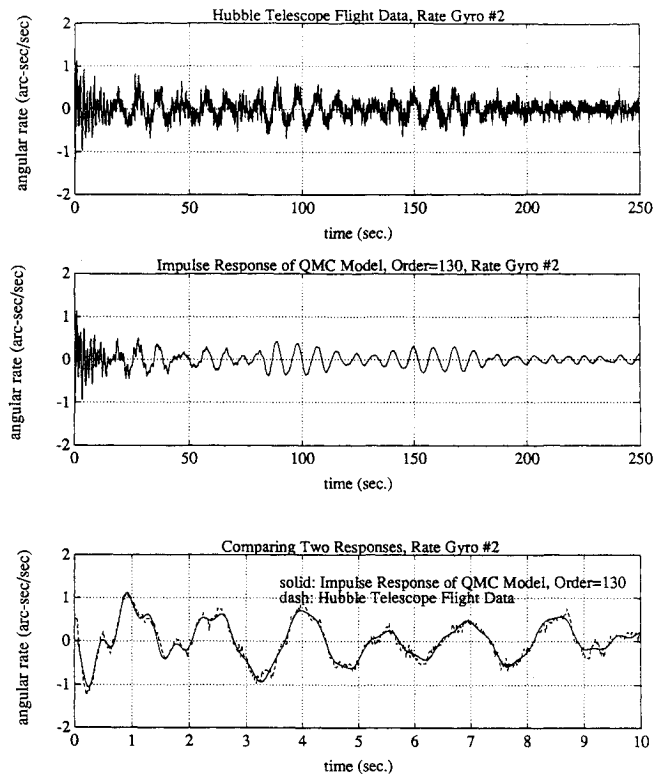

Fig. 8 Q-Markov Cover of the flight data.

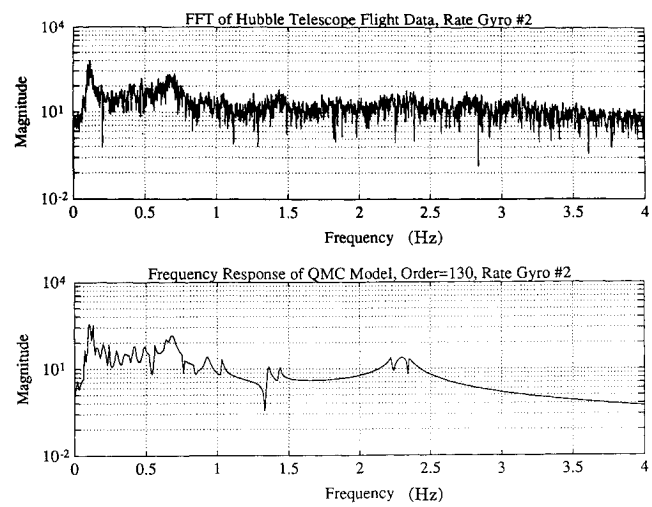

Fig. 9 FFT of the flight data and frequency response of the Q-Markov Cover.

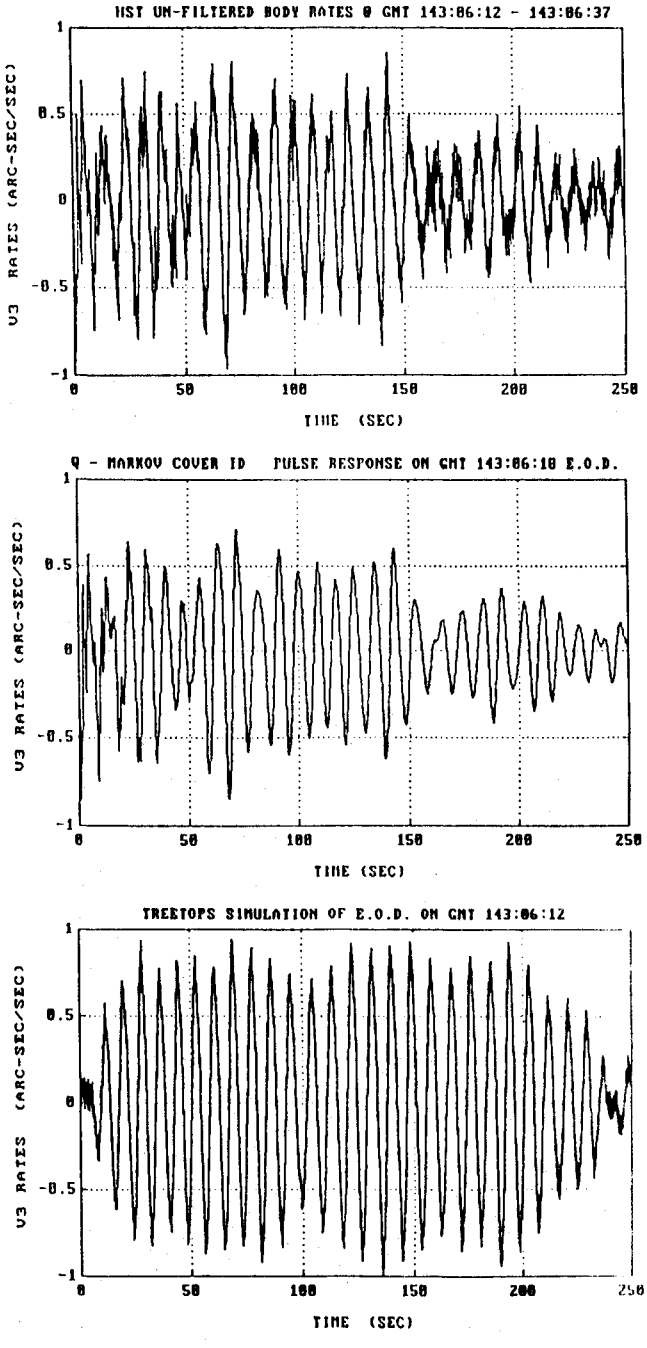

Fig. 9 FFT of he flight data and frequency response of the Q-Markov Cover.

data is very noisy (see Fig. 6). The ε was chosen by trial and error. Modes of the identified model were further analyzed by a technique described in Ref. 10. Some of the noise modes were eliminated to obtain a final high-frequency model.

As discussed in Sec. III, we identified models for systems using each of the four output signals separately with the low-frequency data. The new sampling frequency chosen for the low-frequency data was 4 Hz. $Q = 500$ was chosen for each of these identifications. Again, the ε value was also chosen after several tries. The complete low-frequency model for all four rate gyros was obtained by combining the four single-output Q-Markov Cover models. Balanced model reduction was also applied to the combined single low-frequency models.

The model for the original HST flight data is obtained by combining the high-frequency model (70th order) and the final low-frequency model (100th order). After model reduction, a model of 130th order was produced for the response of the HST to the unknown disturbance. Figure 8 compares a time domain response of the identified model to the flight data. The top plot in the figure shows the response from rate gyro 2 (flight data); the middle plot shows the impulse response from the identified Q-Markov Cover. The first 10 seconds of the data from both plots are superimposed at the bottom of the figure. Note the reasonably good agreement between the model and the data. Figure 9 compares the frequency response of the Q-Markov Cover for rate gyro 2 with flight data. As we can see by examining the flight data, the data contains a large amount of noise. (The presence of the noise can be observed in Fig. 3 before the impulse has occurred and in Fig. 6 as sustained high-frequency oscillations.) The effects of the noise on the obtained Q-Markov Cover were reduced by proper choices of the ε values and by eliminating some noise modes.[10] As a result, the Q-Markov Cover gives a good match to the first 20 seconds of data and has a strong roll-off in magnitude above 2.5 Hz.

From the Q-Markov Cover frequency response (Fig. 9), it is apparent that many modes of the Hubble structure are both excited by (controllable from) the disturbance and measured by (observable in) the rate gyros. The bandwidth of the HST attitude control system, in the maneuver mode, is approximately 0.15 Hz. Within this band, our model has identified four modes that dominate the response. Many of the dominant modes have identified damping ratios less than 1%. During the undisturbed portions of the orbit, the HST high gain controller provides better than the required 0.007 arc-seconds of rms. However, disturbances such as these lead to errors in excess of 0.1 arc-seconds peak, and 0.03 arc-seconds of rms. This explains in part why the attitude control system may have difficulty controlling their vibration. In particular, inadequate models of the disturbance environment led to inadequate disturbance rejection capabilities. Hence, the ability to perform on-orbit system identification should become an operational requirement for this class of space vehicles.

An analytical model was generated by the TREETOPS program.[11] Figure 10 compares the flight data with the Q-Markov Cover and the TREETOPS analytical model of the telescope. The order of the TREETOPS model is 158. The input of the simulation of Q-Markov Cover is a pulse. The input to the TREETOPS model for the simulation is a set of distributed solar array forces that were derived from the same set of flight data. The top plot of Fig. 10 is the flight data for the angular rate of the telescope about vehicle yaw axis ($V3$). The middle plot is the Q-Markov Cover simulation. The bottom plot is the TREETOPS model simulation. The simulation of the identified Q-Markov Cover shows a much better fit to the data than the TREETOPS model. Further investigation should allow improvements in the TREETOPS model to better fit the flight data. However, these models each have distinct advantages. The Q-Markov Cover provides a more accurate reproduction of the measured flight data, but imbeds the disturbance models together with the plant and controller dynamics. Continued research on methods for closed-loop identification will be required to extract the plant model from the closed-loop models.

VI. Conclusion

State-space models of the HST are obtained from flight data by using the Q-Markov Cover identification algorithm. To reduce the computational burden, we partitioned the data into low- and high-frequency components. The response of the identified model is close to the flight data. This analysis revealed many vibration modes within the bandwidth of the attitude control system.

References

[1]Skelton, R. E., and Yousuff, A., "Component Cost Analysis of Large Scale System," *International Journal of Control*, Vol. 37, No. 2, 1983, pp. 285–304.

[2]Wagie, D. A., and Skelton, R. E., "A Projection Approach to Covariance Equivalent Realizations of Discrete Systems," *IEEE Transactions on Automatic Control*, AC-31, 1986, p. 1114.

[3]Villemagne, C., and Skelton, R. E., "Model Reduction Using a Projection Formulation," *International Journal of Control*, Vol. 46, No. 6, 1982, pp. 2141–2169.

[4]Kim, J. H., and Skelton, R. E., "Model Reduction by Weighted Component Cost Analysis," AIAA Dynamics Specialists Conf., Long Beach, CA, April 1990.

[5]Anderson, B. D., and Skelton, R. E., "The Generation of All q Markov Covers," *IEEE Transactions on Circuits and Systems*, Vol. 35, No. 4, 1988, pp. 375–384.

[6]King, A. M., Desai, U. B., and Skelton, R. E., "A Generalized Approach to q-Markov Covariance Equivalent Realizations of Discrete Systems," *Automatica*, Vol. 24, No. 4, 1988, pp. 507–515.

[7]Liu, K., and Skelton, R. E., "Q-Markov Covariance Equivalent Realization Cover and its Application to Flexible Structure Identification," *Journal of Guidance, Control, and Dynamics*, Vol. 16, No. 2, 1993, pp. 308–319.

[8]Moore, B. C., "Principle Component Analysis in Linear Systems: Controllability, Observability, and Model Reduction," *IEEE Transactions on Automatic Control*, Vol. AC-26, No. 1, pp. 17–32.

[9]*Pro-Match User's Manual*, The Math Works, Inc., Aug. 1987.

[10]Liu, K., "Q-Markov Cover Identification and Integrated MCA-OVC Controller Design for Flexible Structures," Ph.D. Dissertation, School of Aeronautics and Astronautics, Purdue Univ., West Lafayette, IN, 1991.

[11]Singh, R. P., VanderVoort, R. J., and Likins, P. W., "Dynamics of Flexible Bodies in Tree Topology—A Computer-Oriented Approach," *Journal of Guidance, Control, and Dynamics*, Vol. 8, No. 5, 1985, pp. 584–590.